AGU ADVANCING EARTH AND SPACE SCIENCE

Geophysical Research Letters®

RESEARCH LETTER
10.1029/2022GL099766

Key Points:

- Approximately three-fifths (59%) of global land area are projected to experience accelerated transition between dry and wet periods
- Southern Asia suffers the most from severe transition between dry and wet periods
- Enhanced precipitation and potential evapotranspiration variabilities contribute to the accelerated dry-to-wet transitions

Supporting Information:

Supporting Information may be found in the online version of this article.

Correspondence to:

S. Wang,
shuo.s.wang@polyu.edu.hk

Citation:

Chen, H., & Wang, S. (2022). Accelerated transition between dry and wet periods in a warming climate. *Geophysical Research Letters*, *49*, e2022GL099766. https://doi.org/10.1029/2022GL099766

Received 26 MAY 2022
Accepted 27 SEP 2022

Author Contributions:

Conceptualization: Shuo Wang
Data curation: Huijiao Chen
Formal analysis: Huijiao Chen, Shuo Wang
Funding acquisition: Shuo Wang
Investigation: Shuo Wang
Methodology: Huijiao Chen
Project Administration: Shuo Wang
Resources: Shuo Wang
Software: Huijiao Chen
Supervision: Shuo Wang
Validation: Huijiao Chen
Visualization: Huijiao Chen
Writing – original draft: Huijiao Chen
Writing – review & editing: Shuo Wang

Accelerated Transition Between Dry and Wet Periods in a Warming Climate

Huijiao Chen[1] and Shuo Wang[1,2]

[1]Department of Land Surveying and Geo-Informatics and Research Institute for Land and Space, The Hong Kong Polytechnic University, Hong Kong, China, [2]Shenzhen Research Institute, The Hong Kong Polytechnic University, Shenzhen, China

Abstract The consecutive occurrence of meteorological dry and wet extremes has been receiving increasing attention due to potentially larger social and environmental impacts than single extremes. However, the changing characteristics of transitions between dry and wet periods remain poorly understood. Here we investigate the dynamic evolution of dry-to-wet transitions in response to climate warming, using the Standardized Precipitation Evapotranspiration Index as well as observations and general circulation models for the periods of 1954–2014 and 2040–2100. We find that approximately three-fifths of global land area are projected to experience an accelerated dry-to-wet transition. Southern Asia has been experiencing the most severe dry-to-wet transitions and is projected to suffer more frequent, more intense, and accelerated dry-to-wet transitions. The increasing potential evapotranspiration (PET) variability plays an important role in accelerating the dry-to-wet transition in Southern Asia, while precipitation and PET variabilities contribute to the intensification of dry-to-wet transitions in Southern North America.

Plain Language Summary The consecutive occurrence of droughts and floods has widespread impacts on agriculture, the ecosystem, and the environment. Here we examine the changes in frequency, intensity, and elapsed time of transitions between dry and wet periods under a warming climate, based on observations and an ensemble of 10 Coupled Model Intercomparison Project Phase 6 climate simulations. We find that approximately 59% of global land area are expected to experience a shorter transition time between dry and wet periods. Southern Asia suffers the most severe dry-to-wet transition. Furthermore, our findings reveal that enhanced potential evapotranspiration (PET) variability contributes to the accelerated transition between dry and wet periods over Southern Asia, and the acceleration of dry-to-wet transitions in Southern North America is associated with an increase in precipitation and PET variabilities as climate warms.

1. Introduction

Hydrometeorological extremes such as droughts and pluvials have significant socio-economic and environmental impacts (De Luca et al., 2020; P. Zhu et al., 2021; Zscheischler et al., 2018). They are expected to become more variable due to anthropogenic climate change (H. Chen, Wang, & Wang, 2020; Martin, 2018; Qing et al., 2022; S. Wang & Wang, 2019), albeit with a large degree of uncertainty (B. Zhang et al., 2019; B. Zhang & Wang, 2021). Severe floods are mainly triggered by persistent and widespread wet spells, also referred to as pluvials (He & Sheffield, 2020). The transition between meteorological dry and wet periods, that is, rapid shift from droughts to pluvials or vice versa, can lead to extreme situations beyond the worst-case scenario expected by emergency managers (De Luca et al., 2020). For instance, the prolonged 2012–2016 California drought followed by the widespread flooding during the winter of 2016–2017 (Folger & Cody, 2017) led to a reduction in crop revenue and a decline in groundwater level, killed millions of forest trees, and caused inconvenience to millions of households (Lund et al., 2018). Such a transition from a dry spell to a wet spell was described as "climate whiplash" or "weather whiplash" (Cohen, 2016; Swain et al., 2018), posing a significant threat to existing emergency response systems (Zscheischler et al., 2020).

Many regions around the world have been affected by the abrupt transition between droughts and pluvials (He & Sheffield, 2020; Zscheischler et al., 2020). A growing body of studies has investigated the spatial co-occurrence or successive occurrence of droughts and deluges or, more generally, dry and wet extremes on local and regional scales across many countries, such as China (H. Chen, Wang, Zhu, & Zhang, 2020; Yan et al., 2013; Yoon et al., 2018), the United States (J. Christian et al., 2015; Yoon et al., 2015), Australia (A. Chen et al., 2021), England and Wales (Parry et al., 2013), even on a global scale (De Luca et al., 2020; He & Sheffield, 2020;

Sun et al., 2020). Previous studies considering dry-wet interactions were conducted with the focus on a specific event (J. Christian et al., 2015) or from a statistical perspective (He & Sheffield, 2020; Sun et al., 2020). The independent disasters were also related to large-scale modes of climate variability such as El Niño–Southern Oscillation (ENSO) (Cohen, 2016; Sun et al., 2020) or directly linked to water variability (Dong et al., 2018; Ford et al., 2021; W. Zhang et al., 2021).

The abrupt transition between dry and wet periods can not only lead to environmental impacts due to nutrient runoff from the agricultural field (Loecke et al., 2017), but also produce acute impacts in unsuspecting and underprepared communities if not detected in advance and communicated with stakeholders and decision-makers (Thompson et al., 2021). Previous studies proposed various methods to detect consecutive extremes with a given temporal window (A. Chen et al., 2021; He & Sheffield, 2020; You & Wang, 2021). Ford et al. (2021) investigated the transition between wet and dry extremes based on the observed yearly SPI range in the Midwest United States over the past 70 years. However, there remains a lack of understanding on the dynamics of the transition between dry and wet periods. Notwithstanding the socio-economic relevance, the dynamic transition between dry and wet periods has seldom been investigated on a global scale. Although previous studies have suggested that precipitation variability is a key factor causing the swing between dry and wet extremes (Dong et al., 2018; Huang & Xie, 2015; Ma et al., 2018; Swain et al., 2018; W. Zhang et al., 2021), little effort has been made to examine the direct linkages between precipitation variability and rapid dry-to-wet transition.

This study aims to provide a comprehensive assessment of historical patterns and future changes in the characteristics of transitions between dry and wet periods globally under a warming climate, based on observations and a Coupled Model Intercomparison Project Phase 6 (CMIP6) ensemble. Furthermore, this study will investigate potential interrelationships of the dry-to-wet transition time, precipitation (P) variability, potential evapotranspiration (PET) variability, and water availability (P–PET) variability. These will have significant implications for understanding physical mechanisms causing the dry-to-wet transition.

2. Data and Methods

2.1. Data and Index

The observed monthly precipitation and PET were derived from the gridded Climate Research Unit Time Series version 4 (CRU TS; Harris et al., 2020) at a 0.5° resolution, and a total of 10 CMIP6 models (Table S1 in Supporting Information S1) were used in this study. The CRU is used as the observation because it is an interpolation of monthly climate anomalies from widespread weather station observations. The historical simulated PET was calculated using the Penman-Monteith method (Allen et al., 1998; Zotarelli & Dukes, 2010), and future simulated PET was calculated using a Modified Penman-Monteith method (Yang et al., 2019) (Text S1 in Supporting Information S1). The modified PET calculation not only takes into account air temperature, relative humidity, wind speed, and solar radiation but also considers the possible CO_2 physiological effect under warmer conditions (Williams et al., 2020; Yang et al., 2019). Our study covers a 61-year baseline period from 1954 to 2014 and a 61-year future period from 2040 to 2100. All datasets were interpolated to a global grid of 144×192. To estimate the statistical robustness, we highlight the regions where the results obtained from at least 70% of CMIP6 models are consistent with each other.

The Standardized Precipitation Evapotranspiration Index (SPEI; Vicente-Serrano et al., 2010) is commonly used to characterize dry and wet conditions at monthly to inter-annual time scales although its primary use is a meteorological drought indicator (Hui-Mean et al., 2018; Su et al., 2018; Sun et al., 2016). The SPEI was calculated using the deviation of monthly precipitation and PET using 3-month aggregated data. The deviation was fitted to a three-parameter log-logistic distribution (The goodness-of-fitness of SPEI distribution is shown in Text S2 in Supporting Information S1) and then was converted to the standard normal distributions (Beguería et al., 2014; McKee et al., 1993; Vicente-Serrano et al., 2010). According to the categories of SPEI, the climatic water condition can be identified as dry (SPEI < -1) and wet (SPEI $> +1$) periods. The selected thresholds are also widely used in previous studies (Hui-Mean et al., 2018; Martin, 2018; Spinoni et al., 2018; Su et al., 2018). In addition, the transition time between dry and wet periods detected by 3-month SPEI has greater significance than those by 1-month SPEI (Text S3 in Supporting Information S1).

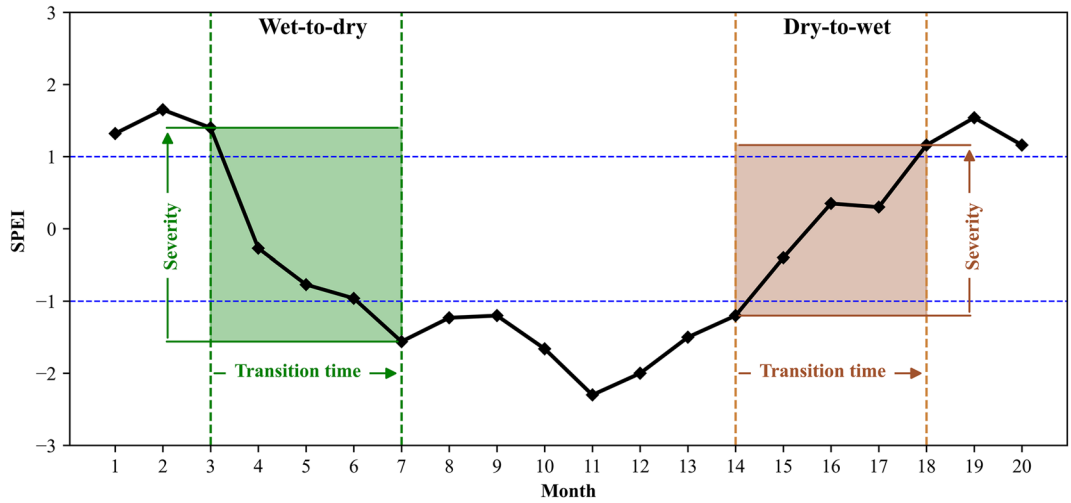

Figure 1. Schematic for the identification of characteristics of (green) a wet-to-dry transition and (brown) a dry-to-wet transition. The black line represents the Standardized Precipitation Evapotranspiration Index value. For example, the dashed brown lines represent the beginning and the end of a dry-to-wet transition, with a duration of 4 months and a severity of 2.36.

2.2. Identification of the Transition Between Dry and Wet Periods

Figure 1 shows two different types of transitions (i.e., wet-to-dry and dry-to-wet transitions), identified by the 3-month SPEI as an example. The dry-to-wet transition begins in the last month in which the SPEI is at or below the threshold of −1 and ends in the first month in which the SPEI is at or above the threshold of +1. It should be noted that we only emphasized the features of dry-to-wet transitions because of the strong spatial and temporal consistency in the characteristics of wet-to-dry and dry-to-wet transitions (Section 3.1).

We define three primary features of dry-to-wet transitions: transition time, intensity, and frequency. As depicted in Figure 1, transition time is defined as the number of months that elapse between the beginning and the end of each transition. Severity is defined as the deviation of SPEI values between the beginning and the end of each transition. Intensity is defined as the ratio of severity to transition time during a transition period. Frequency is defined as the total number of transitions (dry-to-wet or wet-to-dry transitions) that occur in each grid cell for a specific period. The observed characteristics of dry-to-wet transitions were assessed using the CRU data set for a baseline period of 1954–2014. The changes in the transition between dry and wet periods were assessed based on the differences between historical (1954–2014) simulations and future (2040–2100) projections under a high-emission scenario (Shared Socioeconomic Pathway 5–8.5, SSP 5–8.5).

2.3. Transition Event Attribution

To investigate potential climate factors influencing the length of dry-to-wet transition time, the long-term mean seasonal cycle was first removed from the datasets of climate variables (P and PET) by subtracting the climatological monthly mean for each month over the period of 1954–2014. The variability of climate factors was then estimated as the variance of the filtered time series based on a 10-year moving window (Ford et al., 2021; W. Zhang et al., 2021). The transition time of dry-to-wet periods is calculated for each 10-year time window moving forward by one year, generating a sequence of 51-year running variations of transition time from 1954 to 2014 (Ford et al., 2021). The Spearman correlation between transition time and variability of climate variables was also assessed by regression analysis.

3. Results

3.1. Characteristics of the Transition Between Dry and Wet Periods

Figure 2 presents the characteristics of dry-to-wet transitions based on 3-month SPEI on a global scale from 1954 to 2014. A prominent spatial cluster with higher frequency, stronger intensity, and shorter elapsed time of

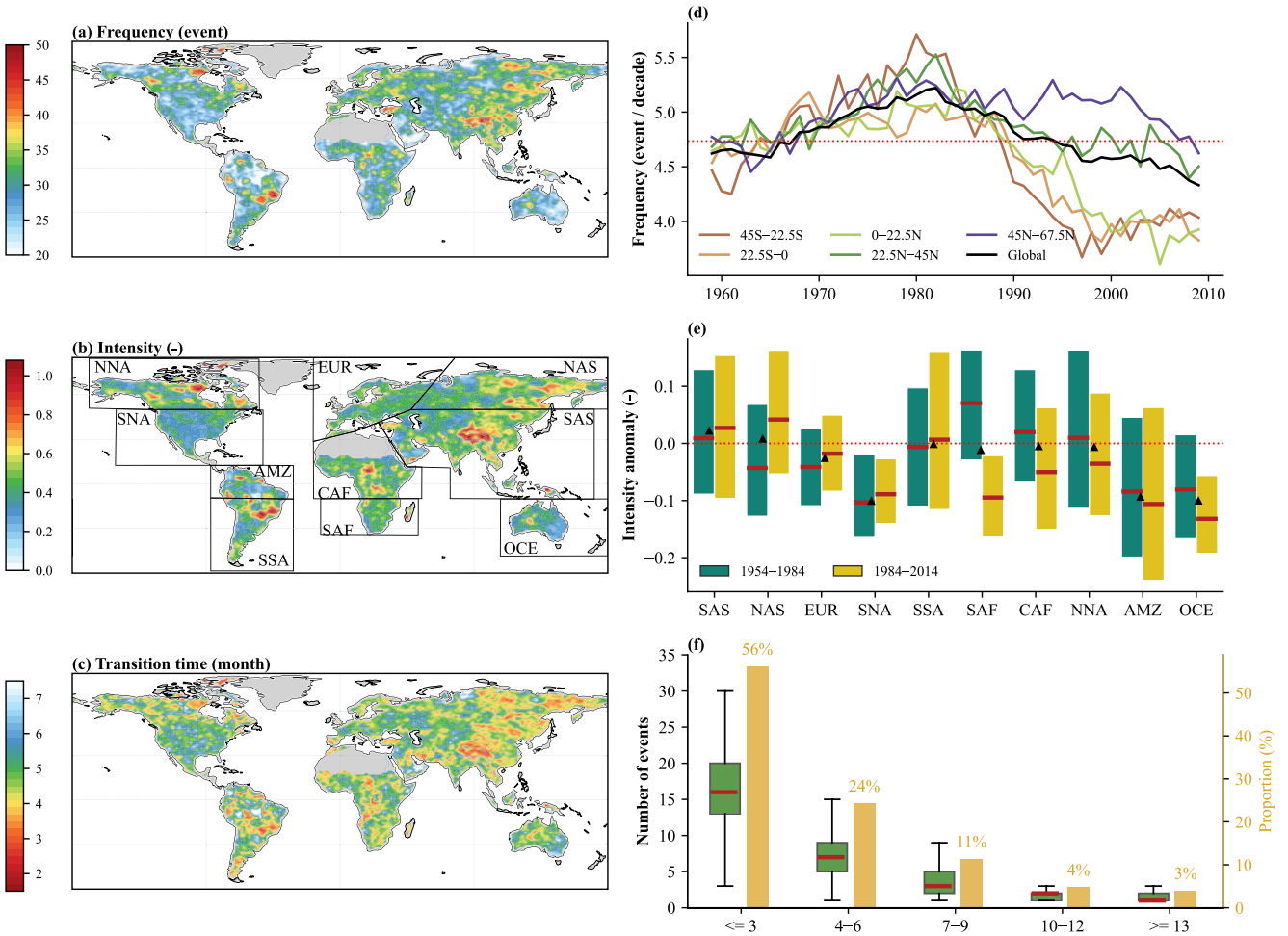

Figure 2. Spatial distributions of (a) average frequency, (b) average intensity (non-dimensional), and (c) average transition time of dry-to-wet transitions. (d) Time series of annual transition frequency with different latitude ranges, derived using a 10-year moving window. (e) Average intensity anomalies across 10 subcontinent regions in the recent 30 years (1984–2014) compared to the preceding 30 years (1954–1984). The red line indicates the median intensity anomalies for a specific period. The black triangle indicates the averaged intensity anomalies for the past 61 years (1954–2014). (f) Average number (green box) and the proportion (yellow bar) of dry-to-wet transitions with different elapsed time scales (≤ 3, 4–6, 7–9, 10–12, and ≥ 13 months). (a–f) Results derived from the Climate Research Unit data set for the historical period of 1954–2014. Note that the reversed color scales represent (c) transition time.

dry-to-wet transitions is found over Eastern Canada, the northern part of the United States, Southeastern Brazil, Central Africa, the majority of Europe, Eastern Asia, and Western Australia. Figure 2d presents the variations of mean dry-to-wet frequency with different latitude ranges. The time series reveal that the dry-to-wet transitions detected in the mid to high latitudes of Northern Hemisphere (45°N−67.5°N) generally have a higher frequency than the southern regions since the late 1980s. The global transition frequency shows a significant increasing trend by the Mann-Kendall test (Tau = 0.82, Slope = 0.028, and $p < 0.001$) from 1954 to 1980s, and a significant decreasing trend (Tau = −0.86, Slope = −0.026, and $p < 0.001$) from 1980 to 2014, which can be explained by the shift of P and PET variabilities in the 1980s (Section 4).

Figure 2e shows the changes in intensity anomalies of dry-to-wet transitions across 10 subcontinent regions in the 1984–2014 period compared to the 1954–1984 period. The box-whisker plots disclose the spatial heterogeneity in the intensity of transition. There is a clear shift from the most intense transitions (1954–1984) to the less intense ones (1984–2014) over Africa (CAF and SAF), which is potentially due to more arid conditions persisting in Africa from the 1980s to the early 21st century (Nicholson et al., 2018; Wainwright et al., 2019). In addition, Eurasia (SAS, NAS, and EUR), Southern North America (SNA), and Southern South America (SSA) have been experiencing more intense transitions. The high frequency and intensity of dry-to-wet transitions occurring in Eurasia, along with dense population and complex climate systems, can lead to high-impact disasters (Thomas

et al., 2013; UNDRR & CRED, 2019). Figure 2f shows the numbers and percentages of dry-to-wet transitions with different transition time scales. It should be noted that the number of dry-to-wet transitions with a rapid transition ($\leq$ 3 months) is largest and occupies 56% of the total number of such transitions. With an increase in transition time, the number of dry-to-wet transitions is likely to decrease.

The characteristics of wet-to-dry transitions are similar to those of dry-to-wet transitions globally, including spatial distributions of transition times (Figures S5 and S6 in Supporting Information S1), temporal variations of frequency (Figure S5c in Supporting Information S1), as well as the numbers and percentages with different transition time scales (Figure S5d in Supporting Information S1). Therefore, we only emphasized the projected changes in the characteristics of dry-to-wet transitions because of the strong spatial and temporal consistency in the characteristics of wet-to-dry and dry-to-wet transitions.

3.2. Projected Changes in Characteristics of Dry-to-Wet Transitions

Figure 3 shows the multi-model ensemble medians of changes in characteristics of dry-to-wet transitions (See Text S4 for historical evaluations of dry-to-wet transitions). The 51% $\pm$ 6% of global land area are projected to experience more frequent dry-to-wet transitions, mainly in the mid-latitude regions including the most parts of the United States and Europe, the southern part of South America, Southeast Asia, and Southeast Australia. The dry-to-wet transition is also expected to become more intense (Figure 3b) over 55% $\pm$ 5% of global land area that mainly cover the regions with high-frequency transitions. Figure 3c shows that approximately 59% $\pm$ 3% of global land area will experience accelerated transitions in the future period of 2040–2100.

To investigate the changes in characteristics of dry-to-wet transitions, Figures 3d–3f show the changes in the frequency, compared with intensity and transition time for each grid point in the CMIP6 multi-model median. As for the changes in frequency versus intensity (Figure 3d), around 44% $\pm$ 4% of grid points are projected to experience more frequent and more intense transitions. In terms of the changes in frequency versus transition time (Figure 3e), approximately 33% $\pm$ 5% of grid points are expected to experience more frequent and more rapid transitions. As for the changes in transition time and intensity (Figure 3f), about 43% $\pm$ 5% of grid points are expected to experience more rapid and more intense transitions. Generally, approximately 32% $\pm$ 5% of global land area are expected to experience more frequent, more intense, and more rapid transitions between dry and wet periods in a warming climate.

Figures 3h and 3g show the multi-model ensemble medians of transition time and intensity assessed for historical and future periods. In terms of transition time, all 10 subcontinent regions are projected to experience accelerated transitions from dry to wet periods (Figure 3h). Specifically, Asia (SAS and NAS) has been suffering intense dry-to-wet transitions (Figure 2e) and is projected to experience more intense transitions in the future. In comparison, North America (NNA and SNA) and Oceania (OCE) have been suffering less intense dry-to-wet transitions (Figure 2e). However, these regions are expected to experience a relative increase in the transition intensity in the future (Figure 3g), which is consistent with previous study (Ford et al., 2021). These suggest an intensified and accelerated transition between droughts and deluges in a changing climate, posing an increasing risk for water management practices. Thus, it is crucial to consider a trade-off between short-term flood control and long-term water storage imperatives to satisfy water demand (He & Sheffield, 2020).

3.3. Contributions of Precipitation and PET Variabilities to Dry-to-Wet Transitions

Large PET variability manifests a rapid rate of soil water from land surface to the atmosphere (Qiu et al., 2021), contributing to the local transition from dry to wet periods. Large precipitation variability yields highly non-uniform precipitation distributions (W. Zhang et al., 2021), and increases the intrinsic likelihood of dry and wet extremes (Swain et al., 2018). During a dry period followed by moderate rainfall events (e.g., low P variability), a sufficient volume of water entering the system may be able to fill the soil column and recover from a substantial degree of antecedent soil drying to a normal period. But for a dry period followed by extreme precipitation events (e.g., large P variability), the extremely large volume of water may be able to quickly saturate the soil column, and even leads to infiltration excess when soils are not yet saturated, increasing the flood risk and entering a wet period (Brunner et al., 2021).

10.1029/2022GL099766

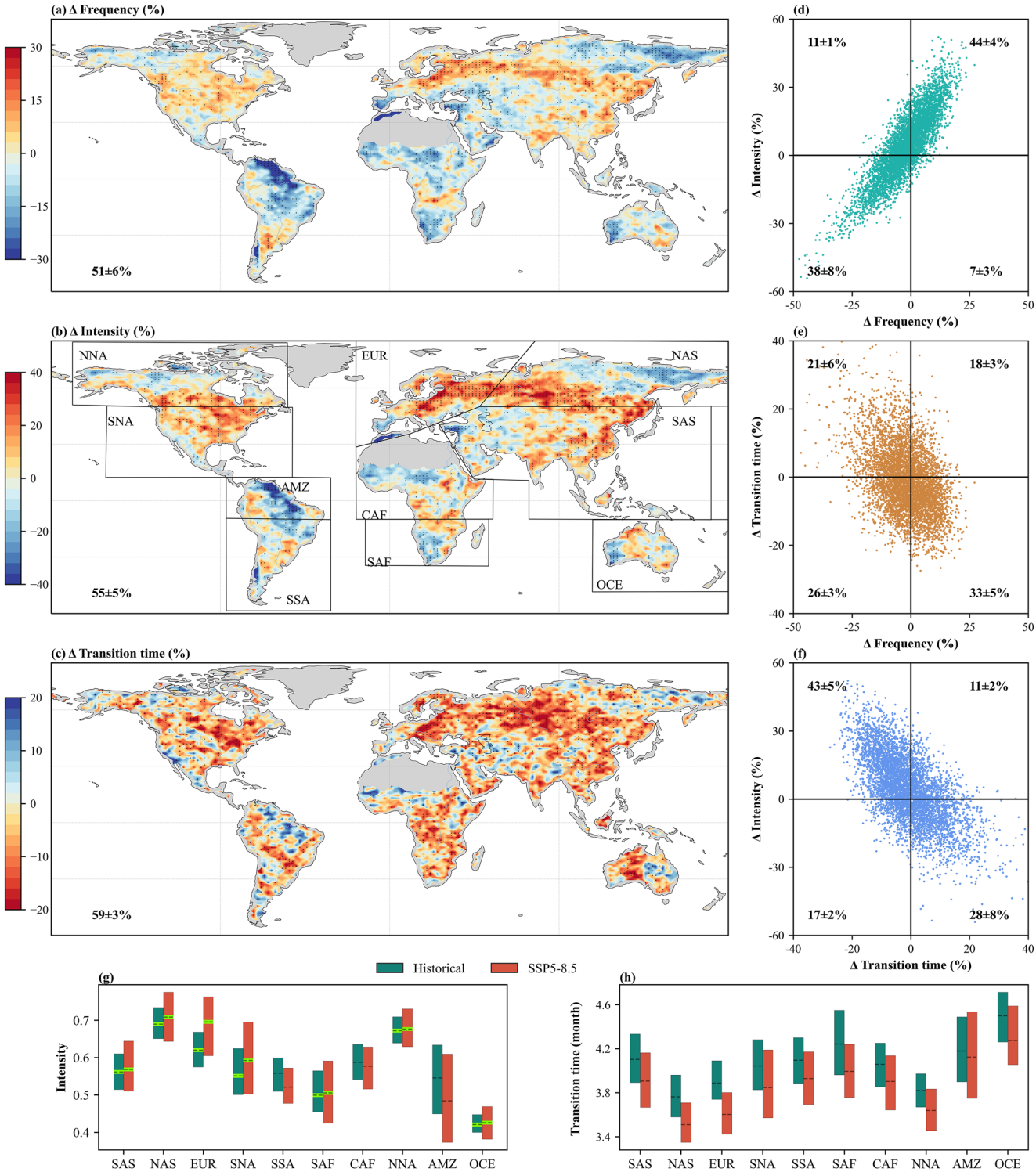

Figure 3. Spatial distributions of Coupled Model Intercomparison Project Phase 6 (CMIP6) multi-model ensemble median changes in (a) frequency, (b) intensity, and (c) transition time of dry-to-wet transitions between the future period of 2040–2100 and the historical period of 1954–2014. The multi-model ensemble medians of the changes in (d) frequency and intensity, (e) frequency and transition time, and (f) transition time and intensity for all grid points. The multi-model ensemble medians of (g) intensity (non-dimensional) and (h) transition time of dry-to-wet transitions across 10 subcontinent regions. (g–h) Bar represents the regional mean changes (ensemble median and 25th to 75th percentile spread), and green line indicates the projected increase in transition intensity across different regions. (a–c) Number represents the fraction of land areas which are projected to experience more frequent, more intense, and more rapid transitions from dry to wet periods. (d–f) Number indicates the fraction of grid points in each quadrant. Note that the reversed color scales represent (c) transition time. Stippling indicates that at least 70% of CMIP6 models agree on the sign of the changes.

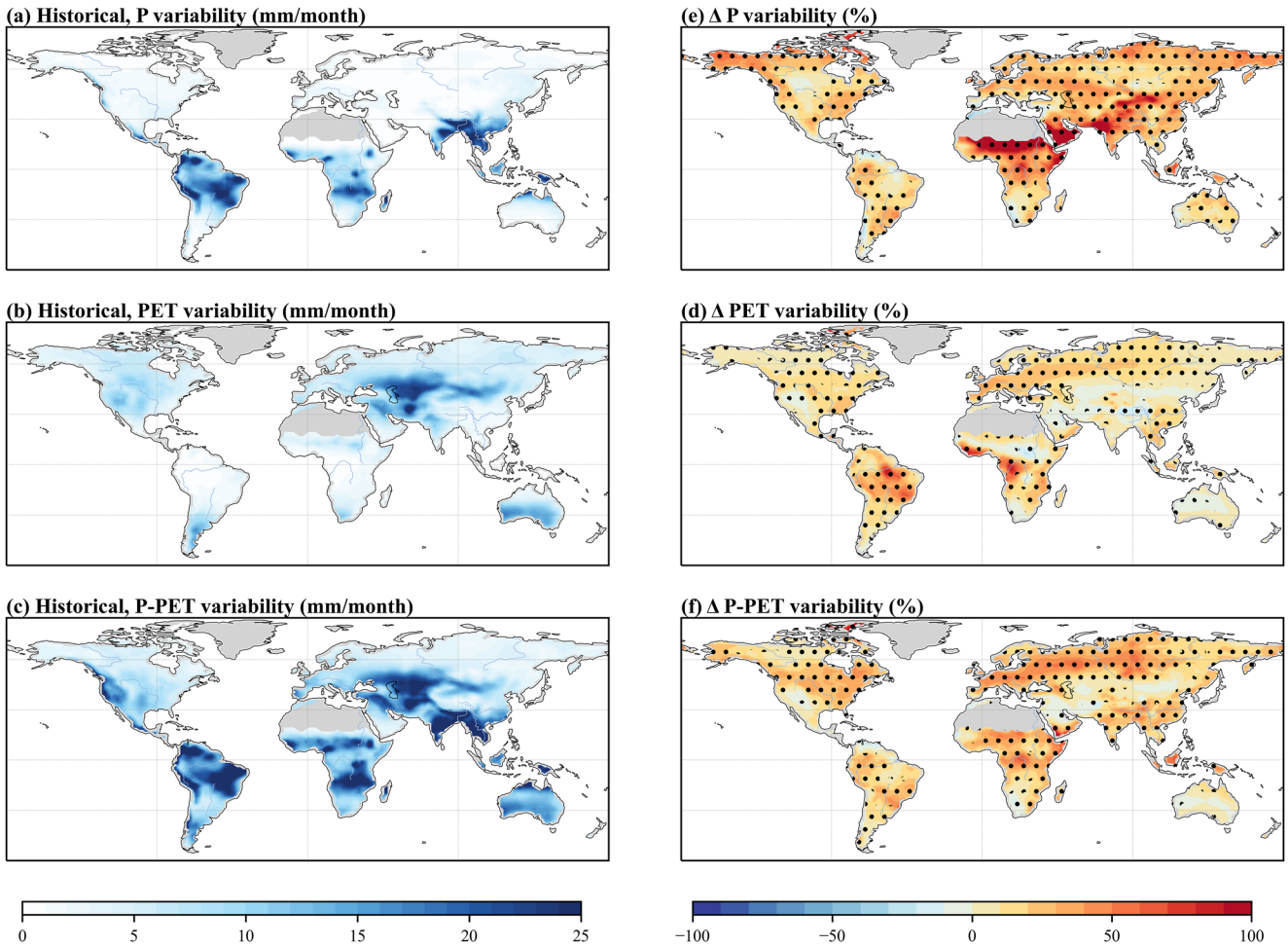

Figure 4. The climatologically values of variabilities of (a) P, (b) potential evapotranspiration (PET), and (c) P–PET for the historical period of 1954–2014 based on the CRU data set. Spatial distributions of Coupled Model Intercomparison Project Phase 6 (CMIP6) multi-model ensemble median changes in the variabilities of (e) P, (d) PET, and (f) P–PET for the future period of 2040–2100 compared to the historical period of 1954–2014. Stippling indicates that at least 70% of CMIP6 models agree on the sign of changes.

We used the Spearman correlation test (Figure S9 in Supporting Information S1) and the random forest model (Text S5 in Supporting Information S1) to assess the interrelationship between variability of climate factors and transition time of dry-to-wet transitions. As for Southern Asia (Figures S9 and S10a in Supporting Information S1), transition time is negatively correlated with PET variability ($r = -0.62$ and $p < 0.05$), while P and P–PET variabilities are not significantly correlated with transition time. Figure S10a in Supporting Information S1 shows strong temporal coherence between PET variability and transition time in Southern Asia. In addition, our findings reveal that PET variability is a more dominant factor influencing the dry-to-wet transition time than P variability (Figure S12 in Supporting Information S1) and a greater PET variability generally corresponds to a shorter transition time in Southern Asia (Figure S13 in Supporting Information S1). In contrast, P variability is stronger negatively correlated with transition time than PET variability over Africa (CAF and SAF), SSA, SNA, and Oceania (OCE) (Figure S9 in Supporting Information S1). Figures S12 and S13 in Supporting Information S1 show that both enhanced P variability and PET variability contribute to the accelerated transition between dry and wet periods over SNA.

As climate warms, the variabilities of P, PET, and P–PET are projected to increase robustly over most global land areas (Figures 4d–4f), with a relatively large increase in P variability in the tropics and little change in PET variability. These signs are consistent with previous studies (Allan et al., 2020; Pendergrass et al., 2017; Seager et al., 2012; W. Zhang et al., 2021). W. Zhang et al. (2021) suggested that the contributions to intensified P variability globally are due to the increasing moisture availability under climate warming and covariation of

moisture and circulation changes. In terms of PET variability, Wang et al. (2022) demonstrated that recent global ET increase is consistent with climate warming based on ground observations. However, the cause of variability in global PET remains unclear. As for P–PET variability, Allan et al. (2020) suggested that increased atmospheric water vapor with warming is a corresponding intensification of horizontal moisture transport, which drives an amplification of P–PET regime.

Increased P variability associated with increased PET variability correspond to shorter transition time between dry and wet periods in North America (NNA and SNA) and Oceania (OCE) (Figure S13 in Supporting Information S1), complementing previous studies with a focus on the contribution of P variability to the transition between dry and wet extremes (Dong et al., 2018; Swain et al., 2018). Thus, the increase in P variability and/or PET variability indicates the fact that the warming climate plays an important role in accelerating transitions between dry and wet periods, leading to a decline in soil moisture memory time scales, especially for deeper soil layers (Lawrence et al., 2007). Thus, a more rapid transition from dry to wet periods may result in reduced warning time, affect vegetation production, and cause more catastrophic consequences beyond expected (Asner et al., 2004; Ford et al., 2021; Sloat et al., 2018). Previous studies pointed out that P is also increasingly partitioned into PET and not into runoff in a warming condition or in arid regions (Zheng et al., 2019), which may further trigger the acceleration of transitions between dry and wet periods.

4. Discussion

The P and/or PET variabilities contribute to the trend shift of the frequency of dry-to-wet transition in the mid-1980s (Figures 2d and S10c). Two factors may contribute to the shift of P/PET variability in the 1980s. The first is a climate regime shift that occurred around the 1980s in different parts of the globe (J. Chen et al., 2008; Reid et al., 2016; Sarkar & Maity, 2021; Z. Zhu, 2018), which manifests itself as sudden jump in several hydroclimatic variables, especially temperature and precipitation (H. Wang, 2001). Large-scale forcing is also an important contributor to the changes in the variabilities of P and PET around the 1980s over global regions. For example, ENSO–related circulation changes have been demonstrated to significantly affect interannual tropical Pacific P variability (Huang & Xie., 2015). Joshi et al. (2022) indicated the integrated effect of Atlantic multidecadal oscillation (AMO) and interdecadal Pacific oscillation (IPO) on P variability over India, leading to P variability shift in the 1980s.

Our findings suggest that P variability and/or PET variability contribute to different impacts on the transition time across different regions: Southern Asia is dominated by PET variability, Africa by P and P−PET variabilities, and Southern Northern America by P and PET variabilities (Figures S9, S12, and S13 in Supporting Information S1). Several factors may contribute to the spatial variation in correlations between variabilities of P/PET/P–PET and dry-to-wet transition time. The first is the role of land–atmosphere coupling in the dry-to-wet development. While the interactions between local P variability and PET variability are very complex, the fundamental relationships between dry-to-wet transition and land–atmosphere couplings can be summarized with key moisture and thermal variables (Pendergrass et al., 2017; Wood et al., 2021; Y. Zhang et al., 2017) in different climatic regions, including energy-limited and water-limited regions. In energy-limited regions, PET variability is mainly controlled by radiative energy, with precipitation playing a relatively minor role (Y. Zhang et al., 2017). It is because lower precipitation corresponds to less cloud coverage and larger radiation, thereby further increasing soil water into the atmosphere. Increased moisture flux from the surface contributes to a wetter atmospheric column, which facilitates the development of dry-to-wet transitions. In water-limited regions, most of evapotranspiration comes from soil evaporation, which is dependent mainly on precipitation (Y. Zhang et al., 2017). Therefore, the dry-to-wet transition is mainly controlled by P variability in water-limited regions. Hence, there are different correlations between dry-to-wet transition time and P/PET variability in different climatic regions.

In addition, climatic features can also influence the different correlations between dry-to-wet transitions and P/PET/P–PET variabilities. In the middle part of Eurasia, the PET variability exceeds 25 mm/month (Figure 4b). By contrast, a majority of land areas in North America experience smaller PET variability in the range between 5 and 10 mm/month compared to Eurasia. Given that larger values of evaporative demand will increase the upper limit for the rate of PET, a dominant PET variability would most likely occur in regions with consistently high PET variability, because a greater potential for rapid increases in evaporative stress on the environment facilitates the dry-to-wet transitions (J. I. Christian et al., 2021). As such, the overall higher importance of PET variability

influencing dry-to-wet transitions in Eurasia (Figure S12 in Supporting Information S1), as compared to North America, may be attributed to climatologically higher values of PET variability in Eurasia. Instead, P and P–PET variabilities dominate the dry-to-wet transitions in Africa and Southern America (Figures 4a and 4c), where both experience climatologically higher values of P and P–PET variabilities than other regions.

It should be noted that the multi-model ensemble climate simulations were used in this study under the highest emission scenario of SSP 5–8.5. The projected changes in the characteristics of dry-wet transitions will vary under different future emission scenarios. In addition, we assessed the transition between dry and wet periods using the 3-month SPEI, but different drought indices might influence the detected patterns in the transition between dry and wet periods. One potential issue with a moving window approach is that the relationship between transition time and variability of climate variables is site and timescale specific, due to differences in climate change velocities (Hoylman et al., 2022).

5. Conclusions

This study investigates historical patterns and future changes in the transition between dry and wet periods on a global scale through observations and 10 CMIP6 climate model simulations. We identify global hotspots of dry-to-wet transitions and explore their dynamic evolution in response to the warming climate. We also examine the interrelationships between characteristics of dry-to-wet transitions and variabilities of P, PET, and water availability (P–PET). These play a crucial role in advancing our understanding of dry-to-wet transition mechanisms and in developing risk mitigation strategies.

Our findings reveal that there will be accelerated transitions from dry to wet periods in most parts of the United States, Europe, the southern part of South America, Southeastern Asia, and Southwestern Australia, with about 59% of global land area under a warming climate. Approximately 32% of global land area are projected to experience more frequent, more intense, and more rapid transitions between dry and wet periods. Southern Asia has been experiencing the most frequent and intense dry-to-wet transitions and it is projected to suffer a further intensification of accelerated transitions. By contrast, SNA has been experiencing less intense transitions; however, it is projected to experience more intense and more rapid transitions from dry to wet periods in a changing climate. The most important factors affecting transition time vary across different regions. Southern Asia is mainly dominated by PET variability, Africa by P variability, and Southern Northern America by P variability and PET variability. Enhanced PET variability contributes to accelerated transition over Southern Asia, while increased variabilities of P and PET may intensify the abrupt alternation between wet and dry periods in Southern North America.

Data Availability Statement

The gridded monthly precipitation and PET are accessible in (a) the Climatic Research Unit Time-Series version 4.00 (CRU TS4.00): https://data.ceda.ac.uk/badc/cru/data/cru_ts/ and (b) the Coupled Model Intercomparison Project Phase 6 (CMIP6): https://esgf-node.llnl.gov/projects/esgf-llnl/. The 3-month SPEI values are available in https://data.mendeley.com/datasets/7s8dhjhg3w.

Acknowledgments
This research was supported by the National Natural Science Foundation of China (Grant 51809223) and the Hong Kong Research Grants Council Early Career Scheme (Grant 25222319).

References

Allan, R. P., Barlow, M., Byrne, M. P., Cherchi, A., Douville, H., Fowler, H. J., et al. (2020). Advances in understanding large-scale responses of the water cycle to climate change. *Annals of the New York Academy of Sciences*, *1472*(1), 49–75. https://doi.org/10.1111/NYAS.14337

Allen, R., Pereira, L., Raes, D., & Smith, M. (1998). Crop evapotranspiration: Guidelines for computing crop water requirements-FAO irrigation and drainage paper 56. *Fao Rome*, *9*, 300.

Asner, G. P., Elmore, A. J., Olander, L. P., Martin, R. E., & Harris, T. (2004). Grazing systems, ecosystem responses, and global change. *Annual Review of Environment and Resources*, *29*(1), 261–299. https://doi.org/10.1146/ANNUREV.ENERGY.29.062403.102142

Brunner, M. I., Swain, D. L., Wood, R. R., Willkofer, F., Done, J. M., Gilleland, E., & Ludwig, R. (2021). An extremeness threshold determines the regional response of floods to changes in rainfall extremes. *Communications Earth & Environment*, *2*(1), 1–11. https://doi.org/10.1038/s43247-021-00248-x

Chen, A., Guan, H., & Batelaan, O. (2021). Seesaw terrestrial wetting and drying between eastern and western Australia. *Earth's Future*, *9*(5), e2020EF001893. https://doi.org/10.1029/2020EF001893

Chen, H., Wang, S., & Wang, Y. (2020). Exploring abrupt alternations between wet and dry conditions on the basis of historical observations and convection-permitting climate model simulations. *Journal of Geophysical Research: Atmospheres*, *125*(9), 1–17. https://doi.org/10.1029/2019JD031982

Chen, H., Wang, S., Zhu, J., & Zhang, B. (2020). Projected changes in abrupt shifts between dry and wet extremes over China through an ensemble of regional climate model simulations. *Journal of Geophysical Research: Atmospheres*, *125*(23), 1–20. https://doi.org/10.1029/2020JD033894

Chen, J., Del Genio, A. D., Carlson, B. E., & Bosilovich, M. G. (2008). The spatiotemporal structure of twentieth-century climate variations in observations and reanalyses. Part II: Pacific pan-decadal variability. *Journal of Climate*, *21*(11), 2634–2650. https://doi.org/10.1175/2007JCLI2011.1

Christian, J., Christian, K., & Basara, J. B. (2015). Drought and pluvial dipole events within the great plains of the United States. *Journal of Applied Meteorology and Climatology*, *54*(9), 1886–1898. https://doi.org/10.1175/JAMC-D-15-0002.1

Christian, J. I., Basara, J. B., Hunt, E. D., Otkin, J. A., Furtado, J. C., Mishra, V., et al. (2021). Global distribution, trends, and drivers of flash drought occurrence. *Nature Communications*, *12*(1), 1–11. https://doi.org/10.1038/s41467-021-26692-z

Cohen, J. (2016). An observational analysis: Tropical relative to Arctic influence on midlatitude weather in the era of Arctic amplification. *Geophysical Research Letters*, *43*(10), 5287–5294. https://doi.org/10.1002/2016GL069102

De Luca, P., Messori, G., Wilby, R. L., Mazzoleni, M., & Di Baldassarre, G. (2020). Concurrent wet and dry hydrological extremes at the global scale. *Earth System Dynamics*, *11*(1), 251–266. https://doi.org/10.5194/esd-11-251-2020

Dong, L., Leung, L. R., & Song, F. (2018). Future changes of subseasonal precipitation variability in North America during winter under global warming. *Geophysical Research Letters*, *45*(22), 12467–12476. https://doi.org/10.1029/2018GL079900

Folger, P., & Cody, B. A. (2017). *Drought in the United States: Causes and current understanding*. Congressional Research Service. Retrieved from http://www.crs.gov

Ford, T. W., Chen, L., & Schoof, J. T. (2021). Variability and transitions in precipitation extremes in the midwest United States. *Journal of Hydrometeorology*, *22*(3), 533–545. https://doi.org/10.1175/JHM-D-20-0216.1

Harris, I., Osborn, T. J., Jones, P., & Lister, D. (2020). Version 4 of the CRU TS monthly high-resolution gridded multivariate climate dataset. *Scientific Data*, *7*(1), 1–18. https://doi.org/10.1038/s41597-020-0453-3

He, X., & Sheffield, J. (2020). Lagged compound occurrence of droughts and pluvials globally over the past seven decades. *Geophysical Research Letters*, *47*(14). https://doi.org/10.1029/2020GL087924

Hoylman, Z. H., Bocinsky, R. K., & Jencso, K. G. (2022). Drought assessment has been outpaced by climate change: Empirical arguments for a paradigm shift. *Nature Communications*, *13*(1), 2715. https://doi.org/10.1038/s41467-022-30316-5

Huang, P., & Xie, S. P. (2015). Mechanisms of change in ENSO-induced tropical Pacific rainfall variability in a warming climate. *Nature Geoscience*, *8*(12), 922–926. https://doi.org/10.1038/ngeo2571

Hui-Mean, F., Yusop, Z., & Yusof, F. (2018). Drought analysis and water resource availability using standardised precipitation evapotranspiration index. *Atmospheric Research*, *201*, 102–115. https://doi.org/10.1016/j.atmosres.2017.10.014

Joshi, M. K., Rai, A., & Kulkarni, A. (2022). Global-scale interdecadal variability a skillful predictor at decadal-to-multidecadal timescales for Sahelian and Indian Monsoon Rainfall. *Npj Climate and Atmospheric Science*, *5*(1), 1–8. https://doi.org/10.1038/s41612-021-00227-1

Lawrence, D. M., Thornton, P. E., Oleson, K. W., & Bonan, G. B. (2007). The partitioning of evapotranspiration into transpiration, soil evaporation, and canopy evaporation in a GCM: Impacts on land–atmosphere interaction. *Journal of Hydrometeorology*, *8*(4), 862–880. https://doi.org/10.1175/JHM596.1

Loecke, T. D., Burgin, A. J., Riveros-Iregui, D. A., Ward, A. S., Thomas, S. A., Davis, C. A., & Clair, M. A. S. (2017). Weather whiplash in agricultural regions drives deterioration of water quality. *Biogeochemistry*, *133*(1), 7–15. https://doi.org/10.1007/s10533-017-0315-z

Lund, J., Medellin-Azuara, J., Durand, J., & Stone, K. (2018). Lessons from California's 2012–2016 drought. *Journal of Water Resources Planning and Management*, *144*(10), 04018067. https://doi.org/10.1061/(ASCE)WR.1943-5452.0000984

Ma, S., Zhu, C., Liu, B., Zhou, T., Ding, Y., & Orsolini, Y. J. (2018). Polarized response of East Asian winter temperature extremes in the Era of arctic warming. *Journal of Climate*, *31*(14), 5543–5557. https://doi.org/10.1175/JCLI-D-17-0463.1

Martin, E. R. (2018). Future projections of global pluvial and drought event characteristics. *Geophysical Research Letters*, *45*(21), 11913–11920. https://doi.org/10.1029/2018GL079807

McKee, T. B., Doesken, N. J., & Kliest, J. (1993). The relationship of drought frequency and duration to time scales. In *Proceedings of the 8th Conference of Applied Climatology, 17-22 January, Anaheim, CA. Preprints, Eighth Conference on Applied Climatology*. American Meteorological Society.

Nicholson, S. E., Funk, C., & Fink, A. H. (2018). Rainfall over the African continent from the 19th through the 21st century. *Global and Planetary Change*, *165*, 114–127. https://doi.org/10.1016/J.GLOPLACHA.2017.12.014

Parry, S., Marsh, T., & Kendon, M. (2013). From drought to floods in England and Wales. *Weather*, *68*(10), 268–274. https://doi.org/10.1002/wea.2152

Pendergrass, A. G., Knutti, R., Lehner, F., Deser, C., & Sanderson, B. M. (2017). Precipitation variability increases in a warmer climate. *Scientific Reports*, *7*, 1–9. https://doi.org/10.1038/s41598-017-17966-y

Qing, Y., Wang, S., Ancell, B. C., & Yang, Z. (2022). Accelerating flash droughts induced by the joint influence of soil moisture depletion and atmospheric aridity. *Nature Communications*, *13*(1), 1139. https://doi.org/10.1038/s41467-022-28752-4

Qiu, J., Shen, Z., Leng, G., & Wei, G. (2021). Synergistic effect of drought and rainfall events of different patterns on watershed systems. *Scientific Reports*, *11*(1), 1–18. https://doi.org/10.1038/s41598-021-97574-z

Reid, P. C., Hari, R. E., Beaugrand, G., Livingstone, D. M., Marty, C., Straile, D., et al. (2016). Global impacts of the 1980s regime shift. *Global Change Biology*, *22*(2), 682–703. https://doi.org/10.1111/gcb.13106

Sarkar, S., & Maity, R. (2021). Global climate shift in 1970s causes a significant worldwide increase in precipitation extremes. *Scientific Reports*, *11*(1), 1–11. https://doi.org/10.1038/s41598-021-90854-8

Seager, R., Naik, N., & Vogel, L. (2012). Does global warming cause intensified interannual hydroclimate variability? *Journal of Climate*, *25*(9), 3355–3372. https://doi.org/10.1175/JCLI-D-11-00363.1

Sloat, L. L., Gerber, J. S., Samberg, L. H., Smith, W. K., Herrero, M., Ferreira, L. G., et al. (2018). Increasing importance of precipitation variability on global livestock grazing lands. *Nature Climate Change*, *8*(3), 214–218. https://doi.org/10.1038/s41558-018-0081-5

Spinoni, J., Vogt, J. V., Naumann, G., Barbosa, P., & Dosio, A. (2018). Will drought events become more frequent and severe in Europe? *International Journal of Climatology*, *38*(4), 1718–1736. https://doi.org/10.1002/joc.5291

Su, B., Huang, J., Fischer, T., Wang, Y., Kundzewicz, Z. W., Zhai, J., et al. (2018). Drought losses in China might double between the 1.5°C and 2.0°C warming. *Proceedings of the National Academy of Sciences of the United States of America*, *115*(42), 10600–10605. https://doi.org/10.1073/pnas.1802129115

Sun, Q., Miao, C., Kouchak, A. A., & Duan, Q. (2016). Century-scale causal relationships between global dry/wet conditions and the state of the Pacific and Atlantic Oceans. *Geophysical Research Letters*, *43*(12), 6528–6537. https://doi.org/10.1002/2016GL069628

Sun, Q., Miao, C., Kouchak, A. A., Mallakpour, I., Ji, D., & Duan, Q. (2020). Possible increased frequency of ENSO-related dry and wet conditions over some major watersheds in a warming climate. *Bulletin of the American Meteorological Society*, *101*(4), E409–E426. https://doi.org/10.1175/BAMS-D-18-0258.1

Swain, D. L., Langenbrunner, B., Neelin, J. D., & Hall, A. (2018). Increasing precipitation volatility in twenty-first-century California. *Nature Climate Change*, *8*(5), 427–433. https://doi.org/10.1038/s41558-018-0140-y

Thomas, V., Albert, J. R. G., & Perez, R. T. (2013). ADB economics working paper series: Climate-related disasters in Asia, (Vol. *358*).

Thompson, P. R., Widlansky, M. J., Hamlington, B. D., Merrifield, M. A., Marra, J. J., Mitchum, G. T., & Sweet, W. (2021). Rapid increases and extreme months in projections of United States high-tide flooding. *Nature Climate Change*, *11*(7), 584–590. https://doi.org/10.1038/s41558-021-01077-8

UNDRRCRED. (2019). An overview of the last 20 years the last 20 years.

Vicente-Serrano, S. M., Beguería, S., & López-Moreno, J. I. (2010). A multiscalar drought index sensitive to global warming: The standardized precipitation evapotranspiration index. *Journal of Climate*, *23*(7), 1696–1718. https://doi.org/10.1175/2009JCLI2909.1

Wainwright, C. M., Marsham, J. H., Keane, R. J., Rowell, D. P., Finney, D. L., Black, E., & Allan, R. P. (2019). 'Eastern African Paradox' rainfall decline due to shorter not less intense Long Rains. *Npj Climate and Atmospheric Science*, *2*(1), 1–9. https://doi.org/10.1038/s41612-019-0091-7

Wang, H. (2001). The weakening of the Asian monsoon circulation after the end of 1970's. *Advances in Atmospheric Sciences*, *18*(3), 376–386. https://doi.org/10.1007/BF02919316

Wang, R., Li, L., Gentine, P., Zhang, Y., Chen, J., Chen, X., et al. (2022). Recent increase in the observation-derived land evapotranspiration due to global warming. *Environmental Research Letters*, *17*(2), 024020. https://doi.org/10.1088/1748-9326/ac4291

Wang, S., & Wang, Y. (2019). Improving probabilistic hydroclimatic projections through high-resolution convection-permitting climate modeling and Markov chain Monte Carlo simulations. *Climate Dynamics*, *53*(3), 1613–1636. https://doi.org/10.1007/s00382-019-04702-7

Williams, A. P., Cook, E. R., Smerdon, J. E., Cook, B. I., Abatzoglou, J. T., Bolles, K., et al. (2020). Large contribution from anthropogenic warming to an emerging North American megadrought. *Science*, *370*(6516), 314–318. https://doi.org/10.1126/SCIENCE.ABF3676

Wood, R. R., Lehner, F., Pendergrass, A. G., & Schlunegger, S. (2021). Changes in precipitation variability across time scales in multiple global climate model large ensembles. *Environmental Research Letters*, *16*(8), 084022. https://doi.org/10.1088/1748-9326/ac10dd

Yan, D. H., Wu, D., Huang, R., Wang, L. N., & Yang, G. Y. (2013). Drought evolution characteristics and precipitation intensity changes during alternating dry-wet changes in the Huang-Huai-Hai River basin. *Hydrology and Earth System Sciences*, *17*(7), 2859–2871. https://doi.org/10.5194/hess-17-2859-2013

Yang, Y., Roderick, M. L., Zhang, S., McVicar, T. R., & Donohue, R. J. (2019). Hydrologic implications of vegetation response to elevated CO_2 in climate projections. *Nature Climate Change*, *9*(1), 44–48. https://doi.org/10.1038/s41558-018-0361-0

Yoon, J. H., Wang, S. Y. S., Gillies, R. R., Kravitz, B., Hipps, L., & Rasch, P. J. (2015). Increasing water cycle extremes in California and in relation to ENSO cycle under global warming. *Nature Communications*, *6*(1), 8657. https://doi.org/10.1038/ncomms9657

Yoon, J. H., Wang, S. Y. S., Lo, M. H., & Wu, W. Y. (2018). Concurrent increases in wet and dry extremes projected in Texas and combined effects on groundwater. *Environmental Research Letters*, *13*(5), 054002. https://doi.org/10.1088/1748-9326/aab96b

You, J., & Wang, S. (2021). Higher probability of occurrence of hotter and shorter heat waves followed by heavy rainfall. *Geophysical Research Letters*, *48*(17), e2021GL094831. https://doi.org/10.1029/2021GL094831

Zhang, B., & Wang, S. (2021). Probabilistic characterization of extreme storm surges induced by tropical cyclones. *Journal of Geophysical Research: Atmospheres*, *126*(3), 1–22. https://doi.org/10.1029/2020JD033557

Zhang, B., Wang, S., & Wang, Y. (2019). Copula-based convection-permitting projections of future changes in multivariate drought characteristics. *Journal of Geophysical Research: Atmospheres*, *124*(14), 7460–7483. https://doi.org/10.1029/2019JD030686

Zhang, W., Furtado, K., Wu, P., Zhou, T., Chadwick, R., Marzin, C., et al. (2021). Increasing precipitation variability on daily-to-multiyear time scales in a warmer world. *Science Advances*, *7*(31), 1–12. https://doi.org/10.1126/sciadv.abf8021

Zhang, Y., Chiew, F. H., Peña-Arancibia, J., Sun, F., Li, H., & Leuning, R. (2017). Global variation of transpiration and soil evaporation and the role of their major climate drivers. *Journal of Geophysical Research: Atmospheres*, *122*(13), 6868–6881. https://doi.org/10.1002/2017JD027025

Zheng, H., Yang, Z. L., Lin, P., Wei, J., Wu, W. Y., Li, L., et al. (2019). On the sensitivity of the precipitation partitioning into evapotranspiration and runoff in land surface parameterizations. *Water Resources Research*, *55*(1), 95–111. https://doi.org/10.1029/2017WR022236

Zhu, P., Abramoff, R., Makowski, D., & Ciais, P. (2021). Uncovering the past and future climate drivers of wheat yield shocks in Europe with machine learning. *Earth's Future*, *9*(5), e2020EF001815. https://doi.org/10.1029/2020EF001815

Zhu, Z. (2018). Breakdown of the relationship between Australian summer rainfall and ENSO caused by tropical Indian Ocean SST warming. *Journal of Climate*, *31*(6), 2321–2336. https://doi.org/10.1175/JCLI-D-17-0132.1

Zotarelli, L., & Dukes, M. (2010). *Step by step calculation of the Penman-Monteith evapotranspiration (FAO-56 method)* (Vol. 1–10). Institute of Food and Agricultural Sciences. Retrieved from https://edis.ifas.ufl.edu/pdffiles/AE/AE45900.pdf

Zscheischler, J., Martius, O., Westra, S., Bevacqua, E., Raymond, C., Horton, R. M., et al. (2020). A typology of compound weather and climate events. *Nature Reviews Earth & Environment*, *1*(7), 333–347. https://doi.org/10.1038/s43017-020-0060-z

Zscheischler, J., Westra, S., Van Den Hurk, B. J. J. M., Seneviratne, S. I., Ward, P. J., Pitman, A., et al. (2018). Future climate risk from compound events. *Nature Climate Change*, *8*(6), 469–477. https://doi.org/10.1038/s41558-018-0156-3

References From the Supporting Information

Akaike, H. (1974). A new look at the statistical model identification. *IEEE Transactions on Automatic Control*, *19*(6), 716–723. https://doi.org/10.1109/TAC.1974.1100705

Anderson, T. W., & Darling, D. A. (1954). A test of goodness of fit. *Journal of the American Statistical Association*, *49*(268), 765–769. https://doi.org/10.1080/01621459.1954.10501232

Beguería, S., Vicente-Serrano, S. M., Reig, F., & Latorre, B. (2014). Standardized precipitation evapotranspiration index (SPEI) revisited: Parameter fitting, evapotranspiration models, tools, datasets and drought monitoring. *International Journal of Climatology*, *34*(10), 3001–3023. https://doi.org/10.1002/joc.3887

Beillouin, D., Schauberger, B., Bastos, A., Ciais, P., & Makowski, D. (2020). Impact of extreme weather conditions on European crop production. *Philosophical Transactions of the Royal Society B*, *375*(1810), 20190510. https://doi.org/10.1098/rstb.2019.0510

Breiman, L. (2001). Random forests. *Machine Learning*, *45*(1), 5–32. https://doi.org/10.1023/a:1010933404324

Das, S., Chakraborty, R., & Maitra, A. (2017). A random forest algorithm for nowcasting of intense precipitation events. *Advances in Space Research*, *60*(6), 1271–1282. https://doi.org/10.1016/J.ASR.2017.03.026

Friedman, J. H. (2001). Greedy function approximation: A gradient boosting machine. *Annals of Statistics*, *29*(5), 1189–1232. https://doi.org/10.1214/AOS/1013203451

Massey, F. J. (1951). The Kolmogorov-Smirnov test for goodness of fit. *Journal of the American Statistical Association*, *46*(253), 68–78. https://doi.org/10.1080/01621459.1951.10500769

Shapiro, S. S., & Wilk, M. B. (1965). An analysis of variance test for normality (complete samples). *Biometrika*, *52*(3–4), 591–611. https://doi.org/10.1093/BIOMET/52.3-4.591

Singh, J., Ashfaq, M., Skinner, C. B., Anderson, W. B., Mishra, V., & Singh, D. (2022). Enhanced risk of concurrent regional droughts with increased ENSO variability and warming. *Nature Climate Change*, *12*(2), 163–170. https://doi.org/10.1038/s41558-021-01276-3

Stagge, J. H., Tallaksen, L. M., Gudmundsson, L., Van Loon, A. F., & Stahl, K. (2015). Candidate distributions for climatological drought indices (SPI and SPEI). *International Journal of Climatology*, *35*(13), 4027–4040. https://doi.org/10.1002/JOC.4267

Stephens, M. A. (1974). EDF statistics for goodness of fit and some comparisons. *Journal of the American Statistical Association*, *69*(347), 730–737. https://doi.org/10.1080/01621459.1974.10480196

Wang, H., Chen, Y., Pan, Y., Chen, Z., & Ren, Z. (2019). Assessment of candidate distributions for SPI/SPEI and sensitivity of drought to climatic variables in China. *International Journal of Climatology*, *39*(11), 4392–4412. https://doi.org/10.1002/joc.6081

Yang, Y., Zhang, S., Roderick, M. L., McVicar, T. R., Yang, D., Liu, W., & Li, X. (2020). Comparing palmer drought severity index drought assessments using the traditional offline approach with direct climate model outputs. *Hydrology and Earth System Sciences*, *24*(6), 2921–2930. https://doi.org/10.5194/hess-24-2921-2020